International Journal of Mass Spectrometry 285 (2009) 70–77

Contents lists available at ScienceDirect

International Journal of Mass Spectrometry

journal homepage: www.elsevier.com/locate/ijms

Structural characterization of negatively charged glycosaminoglycans using high-energy (50–150 keV) collisional activation

Christopher J. Taylor[a], Ruth M. Burke[a], Bohan Wu[a], Subhasis Panja[b], Steen Brøndsted Nielsen[b], Caroline E.H. Dessent[a,*]

[a] Department of Chemistry, University of York, Heslington, York YO10 5DD, UK
[b] Department of Physics and Astronomy, Aarhus University, Ny Munkegade, DK-8000 Aarhus, Denmark

ARTICLE INFO

Article history:
Received 25 March 2009
Received in revised form 24 April 2009
Accepted 27 April 2009
Available online 3 May 2009

Keywords:
Glycosaminoglycan
Multiply charged anions
Sulphated sugars
Collision-induced dissociation
High-energy mass spectrometry

ABSTRACT

Anionic glycosaminoglycan mono- and disaccharides (IVA, IH and IS) were subjected to very high-energy collisions (50–150 keV ion kinetic energy prior to collision) with Neon gas in an accelerator mass spectrometer, to explore the possibility of using this method to structurally characterize anionic sugars. Experiments were also conducted for the $Na^+ \cdot IH^{2-}$ and $Na^+ \cdot IS^{3-}$ sodiated complexes. This high-energy ion collision technique is applied here to sugars for the first time. Low-energy collision-induced dissociation (CID) measurements obtained using resonance excitation in a quadrupole ion-trap are presented for comparison. The high-energy measurements produce a rich variety of fragment ions, illustrating the general utility of the technique for providing detailed information for structurally characterizing sugar ions. We discuss the observed fragmentation patterns with reference to the known fragmentation behavior of small gas-phase monoanions, multiply charged anions and cation-dianion complexes.

1. Introduction

Over recent years, the study of gas-phase biological molecules has developed into a rapidly expanding field of research, with considerable experimental and theoretical effort being expended to provide detailed insights into the geometric and electronic properties of isolated biomolecules [1–11].

Progress in this area has been made possible by the application of generic chemical physics techniques to biomolecular systems, in particular through the application of high-resolution laser spectroscopy [1,4–10]. While laser spectroscopy is particularly powerful at providing detailed geometric structures, there is also scope for applying other molecular physics techniques in this area [11–14]. In this work, we describe the application of a high-energy ion-collision technique to the structural characterization of gas-phase sugar molecules.

Glycosaminoglycans (GAGs) are linear, sulfated polysaccharides found on the cell surfaces of a wide range of organisms. GAGs have been implicated in numerous biological roles including cell signaling, cancer progression, and in the regulation of the inflammatory immune response [15]. Although GAGs are unbranched and composed of repeating chains of acidic and basic sugar subunits, their structure is complex due to the varying levels of sulphation and N-acetylation. Heparin and Heparan Sulphate are the most intensively studied GAGs and are composed of a repeating disaccharide subunit made up of hexuronic acid followed by glucosamine. The structural complexity of heparins arises through several factors, including whether the hexuronic acid is either a glucuronic or an iduronic acid, and the positions of sulphation and acetylation [15].

In this study, we explore the possibility of structurally characterizing anionic GAGs by performing electron detachment *via* very high-energy collisions (50–150 keV ion kinetic energy prior to collision) with a nobel gas. This high-energy collision technique has previously been applied to studying the structures and potential energy surfaces of a number of gas-phase chemical systems, [16–21] including multiply charged oligonucleotide anions, [20] but is applied here to sugars for the first time. We also present low-energy collision-induced dissociation (CID) measurements obtained using resonance excitation in a quadrupole ion-trap for comparison, since low-energy CID is widely used to characterize the structures of oligosaccharides. Fig. 1 illustrates the acidic sugars that have been investigated in this initial study, including three prototypical GAG disaccharides (IVA, IH and IS), and three monomer sugar units (which we label A, B and C). These sugars are deprotonated in solution, so that negative ion electrospray ionization produces deprotonated gas-phase anions. The selected sugars are more densely charged than the related systems that have been studied previously using lower energy activated dissociation [22–24].

* Corresponding author. Tel.: +44 1904 434092; fax: +44 1904 432516.
E-mail address: ced5@york.ac.uk (C.E.H. Dessent).

1387-3806/$ – see front matter © 2009 Elsevier B.V. All rights reserved.
doi:10.1016/j.ijms.2009.04.009

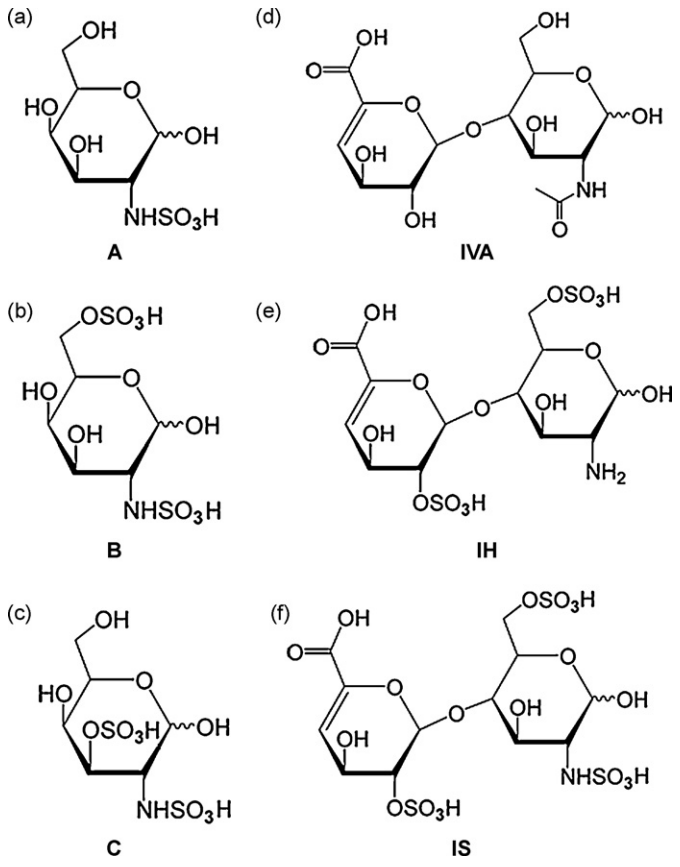

Fig. 1. The chemical structures of the six sulphated sugars studied in this work. (a) The A monosaccharide, GlcNS, (b) the B monosaccharide, GlcNS-6S, (c) the C monosaccharide, GlcNS-3S, (d) the IVA disaccharide, α-ΔUA-[1 → 4]-GlcNAc, (e) the IH trianionic disaccharide, α-ΔUA-2S-[1 → 4]-GlcN-6S, and (f) the IS disaccharide, α-ΔUA-2S-[1 → 4]-GlcNS-6S. (The sugar names have been abbreviated as follows: ΔUA = 4-deoxy-L-threo-hex-4-enopyranosyluronic acid; GlcN = D-glucosamine; Ac = Acetyl; NS, 2S, 3S and 6S = N-sulfo, 2-sulfate, 3-sulfate and 6-sulfate, respectively.)

Determining the pattern of sulphate and acetylate substitution displayed on Heparin and Heparan Sulphate is a matter of particular biological importance as it is thought to be the key to their biochemical activity. The availability of samples is limited to naturally occurring species since GAGs cannot yet be routinely synthesized. For this reason, structural characterization by NMR is severely limited by the purity and volume of material available [25]. Enzymatic digestion and Capillary Electrophoresis/MS^n based characterization techniques suffer from high sample consumption, low turnaround times, and low accuracy relative to mass spectrometry techniques, hence limiting the structural information that can be obtained from these methods [26]. A full complement of cross-ring and glycosidic cleavage fragments is required to determine the sequence of the sugar polymer and the sulphation sites within the sugar units. The suitability of mass-spectral techniques for obtaining structural information on GAG systems is therefore strongly dependent on the method's ability to retain the fragile sulphate groups following molecular fragmentation.

Recent advances in the structural characterization of anionic saccharides have included the application of Electron Detachment Dissociation (EDD) to effect the fragmentation of GAG tetrasaccharides [22,23]. This method involves the irradiation of a multiply charged anionic GAG with electrons of 15–20 eV, initiating electron detachment and subsequent fragmentation. Analysis of the resulting products has revealed the presence of fragments not seen by either low-energy CID or infrared multi-photon dissociation (IRMPD) techniques, and has shown an abundance of cross-ring and glycosidic cleavages. In addition, EDD was shown to be capable of distinguishing between the epimers iduronic and glucuronic acid based on the fragments produced [23]. To date however, experiments have been limited to model tetrasaccharides containing a lower level of sulfation than has been seen previously in biologically active GAG chains. We anticipate that high-energy ion collisions may also lead to EDD-type fragmentation of sugars and may therefore prove highly useful for performing structural characterization of GAGs.

2. Experimental

2.1. Mass-analyzed ion kinetic energy (MIKE) spectrometry

The experimental set-up of the SEP 1 accelerator mass spectrometer has been described in detail previously [17]. Monosaccharides (Dextra Laboratories) and disaccharides (Sigma–Aldrich) were purchased as the sodium salt complexes. All compounds were used without further purification. The ions studied were prepared *via* ESI (negative ion mode) from 1:1 water–methanol solutions. The sugars studied were mass selected in the following charge states, A^-, B^{2-}, C^{2-}, IVA^-, IH^{2-} and IS^{3-}, where we denote A^- to be equivalent to the more commonly used $[A-H]^-$, etc., to simplify the labeling of the fragmentation mass spectra.

Accelerated ions of 50 keV (monoanions), 100 keV (dianions) and 150 keV (trianions) kinetic energy were mass selected by a magnet, and subjected to single-collision activation in a 3 cm collision cell containing neon gas at a pressure of approximately 0.2 mTorr. Mass analyzed ion kinetic energy scans of the anions exiting the collision cell were recorded using a 180° hemi-spherical electrostatic analyzer coupled to a channeltron detector. The flight time from the collision cell to the detector is a few microseconds, setting a limit on the time available for rearrangement of the parent or fragment ions following collision. We note that due to the design of the detector on the SEP1 instrument, a peak is present below the parent ion. For dianionic species, this means that artificial peaks can mask the presence of (dianionic) fragment ions corresponding to loss of a neutral water unit from the parent ion.

2.2. Low-energy collision-induced dissociation

A Finnigan LCQ electrospray quadrupole ion-trap mass spectrometer in negative ion mode was used to perform the low-energy CID experiments as described previously [27]. Sample solution concentrations were 10^{-4} M in methanol, prior to electrospraying in an 80:20 methanol/water solution. Signal optimization was performed using the LCQ automated tuning feature with the cone voltage set at 4.2 kV and a capillary temperature of 150 °C. The sample flow rate was set to 5 μL/min.

Low-energy CID (or resonance excitation) was performed by applying an AC excitation voltage to the end caps of the ion trap. The LCQ uses a Mathieu q_z value of 0.25 and an excitation time of 30 ms. This induces multiple low-energy collisions with the Helium background gas (1×10^{-4} Torr) at a rate of $\sim 10^4\ s^{-1}$. When the high-energy tail of the ion energy envelope reaches the activation energy for the lowest energy decomposition pathway, fragment ions are observed [28]. The excitation voltage applied is varied between 0 and 2.5 V to optimize the number of product fragment ions for each sample, with CID energies being quoted as a percentage of the 2.5 V excitation voltage in line with standard practice [29,30].

3. Results

In this work, we adopt the fragment labeling scheme proposed by Domon and Costello to describe the fragmentation patterns of the dissacharide ions [31]. We extend this scheme to label the cross-ring fragmentations of the monosaccharide anions. The labeling scheme is illustrated in Fig. 2.

3.1. Monosaccharides

The low-energy CID fragmentation mass spectrum of the A^- (GlcNS) monoanionic monosaccharide (m/z = 258) is displayed in Fig. 3a (CID energy = 11.5%). The major fragment ion at m/z = 138 is assigned to the $^{0,2}X_0^-$ fragment (*i.e.*, A^--$^{0,2}A_1$). A second fragment ion peak is present at m/z = 240, representing loss of a neutral water molecule from the parent ion. Such fragments are a common feature of negative-ion Heparin mass spectra [32].

Fig. 3b displays the high-energy MIKE fragmentation spectrum of A^-. The number of fragment ions produced following high-energy collisional excitation is considerably increased compared to the low-energy CID spectrum (Fig. 3a), even for this relatively simple molecular ion. As in the low-energy CID spectrum, $^{0,2}X_0^-$ is the major fragment ion in the MIKE spectrum. The presence of this fragment is consistent with the sulphate group carrying the negative charge in the parent ion. The pair of peaks at m/z = 80.3 and m/z = 97 are assigned to the SO_3^- and HSO_4^- fragment ions, since this pair of ions are commonly observed in the low-energy CID of sulphated GAGs [32]. The appearance of the SO_3^- and HSO_4^- fragment-ion pair strongly indicates that the excess charge is located on the sulphate group in the parent ion.

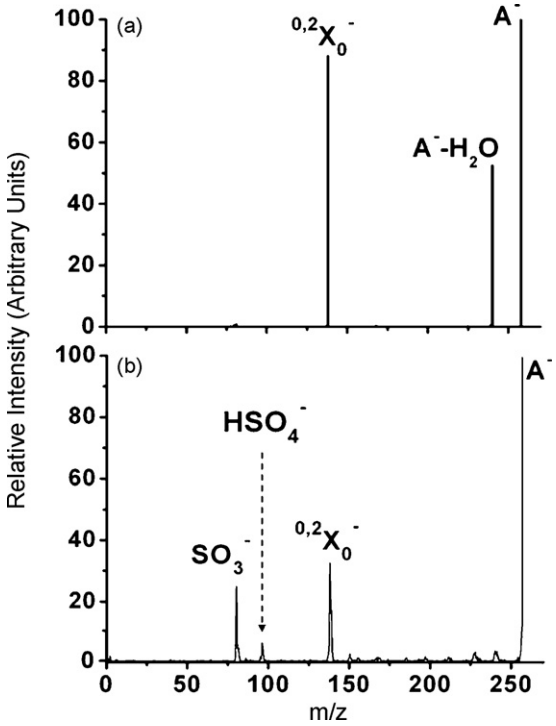

Fig. 3. (a) Low-energy CID mass spectrum of the A^- (*i.e.*, $[A–H]^-$) monanionic monosaccharide at 11.5% collision energy. (b) Negative-ion MIKE spectrum (50 keV) following high-energy collision of A^- with Neon.

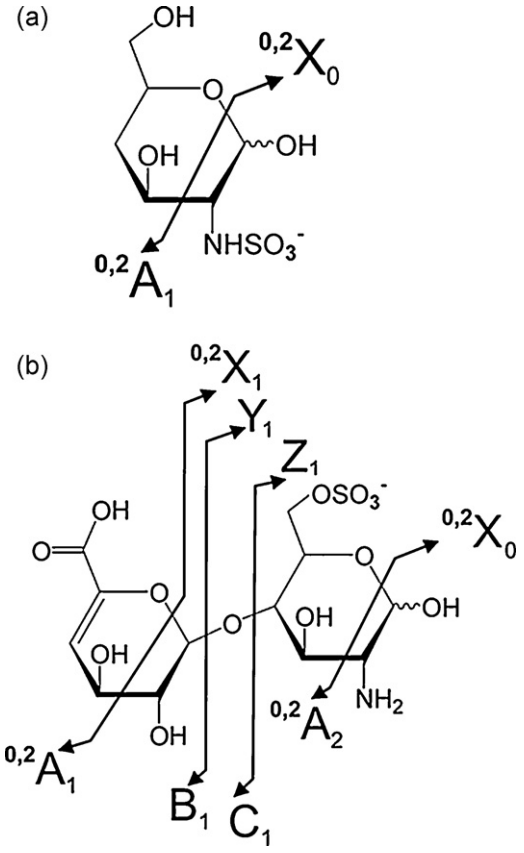

Fig. 2. Fragment labeling scheme used in this work for (a) monosacharides and (b) disaccharides. (This follows the scheme of Domon and Costello [31].) The A, B and C labels are used to indicate a fragment containing a non-reducing end of the GAG, while X, Y and Z denote fragments which include the reducing end of the sugar. (The reducing end is defined as the ring with a C_1 carbon not involved in a glycosidic bond.)

Fig. 4a shows the low-energy CID fragmentation mass spectrum of the B^{2-} (GlcNS-6S) dianionic monosaccharide (CID energy = 5%). The low-energy fragmentation behavior of B^{2-} mirrors that of other

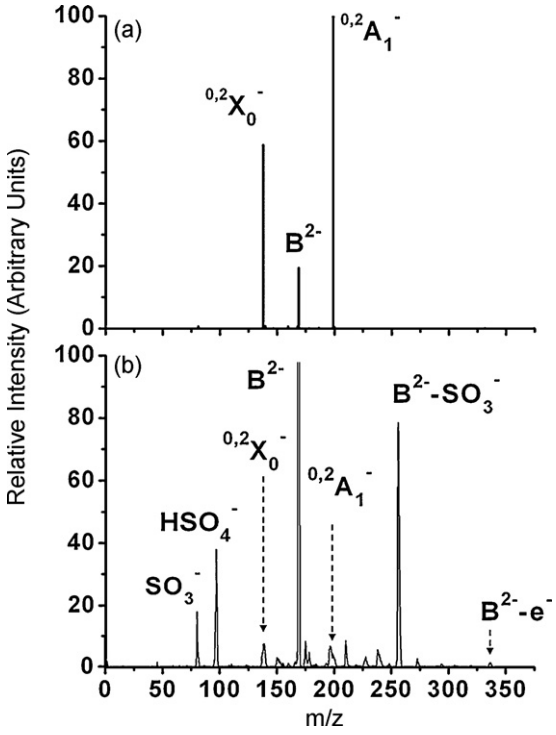

Fig. 4. (a) Low-energy CID mass spectrum of the B^{2-} (*i.e.*, $[B–2H]^{2-}$) dianionic monosaccharide at 5% collision energy. (b) Negative-ion MIKE spectrum (100 keV) following high-energy collision of B^{2-} with Neon.

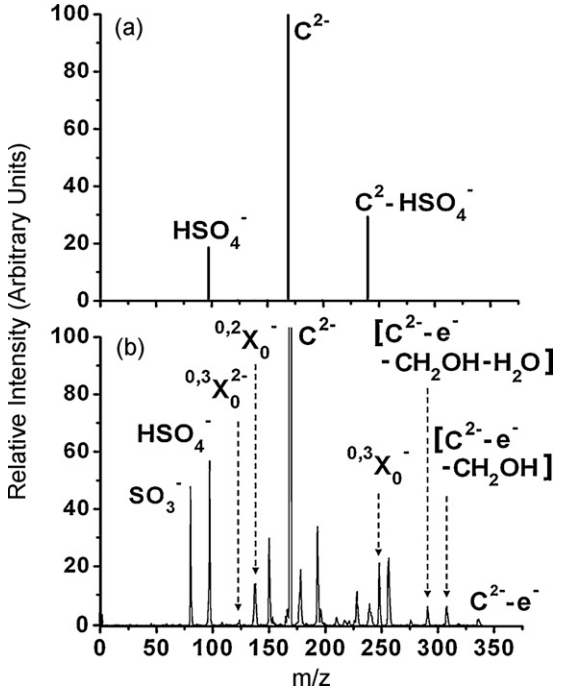

Fig. 5. (a) Low-energy CID mass spectrum of the C^{2-} (*i.e.*, $[C-2H]^{2-}$) dianionic monosaccharide at 6% collision energy. (b) Negative-ion MIKE spectrum (100 keV) following high-energy collision of C^{2-} with Neon.

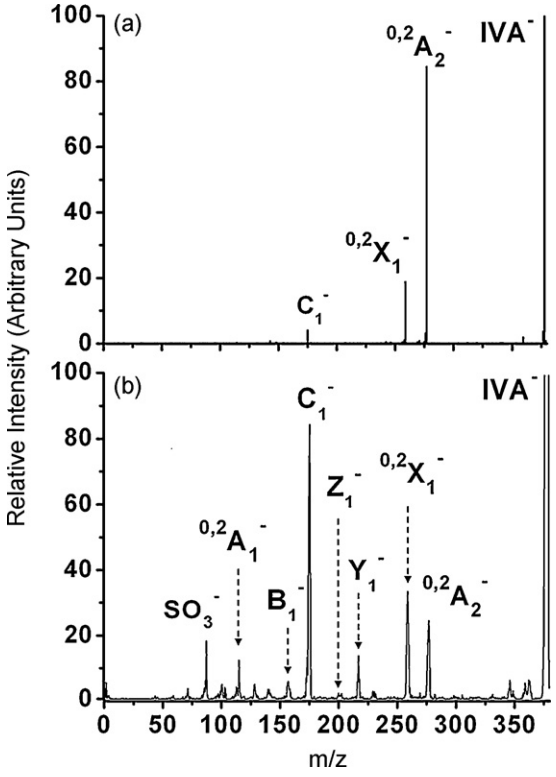

Fig. 6. (a) Low-energy CID mass spectrum of the IVA^- (*i.e.*, $[IVA-H]^-$) monoanionic disaccharide at 10.5% collision energy. (b) Negative-ion MIKE spectrum (50 keV) following high-energy collision of IVA^- with Neon.

small molecular dianions, since it undergoes ionic fragmentation (or *Coulomb explosion*) with the production of two monoanionic species [28,33,34,35]. These fragment ions are assigned as $^{0,2}X_0^-$ (m/z = 138) and $^{0,2}A_1^-$ (m/z = 199), corresponding to a cross-ring fragmentation. It is notable that the dianionic B^{2-} fragments more efficiently at a lower CID energy than the monanionic A^-, in line with the lower intrinsic stability of multiply charged ions [33].

The high-energy MIKE fragmentation spectrum of B^{2-} (100 keV) is displayed in Fig. 4b. The number of fragment ions produced following high-energy collisional excitation is again considerably increased compared to the low-energy CID spectrum (Fig. 4a). The most prominent fragment ion peak (m/z = 256) corresponds to ionic fragmentation of the parent ion with loss of SO_3^-. As in the low-energy CID spectrum, B^{2-} again fragments across the saccharide ring with production of the $^{0,2}X_0^-$ and $^{0,2}A_1^-$ monoanions. The SO_3^- and HSO_4^- pair of fragments are also again evident in the MIKE spectrum, consistent with the excess charges being carried by the sulfate and aminosulfate groups in the parent ion [32]. Loss of water is a common fragmentation channel, with several peaks in the MIKE spectrum of B^{2-} being assigned to loss of water from either the parent or product ions. One of the most striking features of the B^{2-} high-energy fragmentation spectrum is the very low intensity of the electron detachment ion, *i.e.*, $B^{2-}-e^-$. This contrasts with the high-energy fragment spectra of other molecular dianions, *e.g.*, deprontonated oligonucletides, where the major fragment ion typically corresponds to electron detachment from the parent dianion [16–21]. We note that parent ion $-SO_3^-$ fragment ion (m/z = 256) may also result from initial electron loss, followed by loss of neutral SO_3. This point will be discussed further in the discussion section.

The low-energy CID fragmentation mass spectrum of the C^{2-} (GlcNS-3S) dianionic monosaccharide (m/z = 169) is displayed in Fig. 5a (CID energy = 6%). C^{2-} again fragments efficiently at a relatively low CID energy, consistent with the intrinsic instability of small gas-phase dianions. Low-energy fragmentation of C^{2-} again proceeds *via* ionic fragmentation (*Coulomb explosion*) of the dianion, although this time with production of the HSO_4^- and $[C^{2-}-HSO_4^-]^-$ pair of monoanions. This fragmentation pattern is notably different from that of B^{2-}, where ionic fragmentation occurred with cross-ring fragmentation, and reflects the fact that the two excess charges are held on adjacent position on the C^{2-} sugar ring.

The high-energy MIKE fragmentation spectrum of C^{2-} (100 keV) shown in Fig. 5b, exhibits similar fragmentation products to the corresponding spectrum of B^{2-}, consistent with the C^{2-} dianion fragmenting *via* Coulomb explosion upon high-energy collision. The SO_3^- and HSO_4^- pair of fragments is again prominent, consistent with the excess charges being carried by the sulfate and aminosulfate groups in the parent ion [32]. The $^{0,2}X_0^-$ fragment is present, and both the singly and doubly charged $^{0,3}X_0^{n-}$ ($n = 1, 2$) ions are present. (The corresponding A^- fragments may be absent due to electron loss during or after the high-energy collision.) Fragments corresponding to loss of CH_2OH and H_2O units for either the parent ion or the product ions are common (Table 1). The fragment ion corresponding to electron detachment from the parent ion, *i.e.*, $C^{2-}-e^-$ (m/z = 337), again appears with low intensity, although for C^{2-} it is also accompanied by loss of CH_2OH and $CH_2OH + H_2O$. A full list of the fragments observed in the low- and high-energy fragmentation spectra for the three monosaccharides studied is given in Table 1, with assignments.

3.2. Disaccharides

Fig. 6a displays the low-energy fragmentation mass spectrum of the IVA^- monoanionic disaccharide (α-ΔUA-[1 → 4]-GlcNAc) obtained at 10.5% CID energy. IVA^- is distinctive amongst the sugars investigated in this study, since the excess charge cannot be held on a sulphate group. The most prominent fragment ions result from cross-ring cleavages of each sugar ring, producing $^{0,2}A_2^-$ and $^{0,2}X_1^-$. A C_1^- fragment ion associated with Z cleavage is evident at

Table 1
Fragment ions present in the low- and high-energy fragmentation spectra for the A^-, B^{2-} and C^{2-} monosaccharide anions[a].

Parent Ion	Low-energy fragment ions	High-energy fragment ions
A^-	$^{0,2}X_0^-$ (138, **100%**), $A^- - H_2O$ (240, **60%**)	$^{0,2}X_0^-$ (138, **100%**), SO_3^- (80, **77%**), HSO_4^- (97, **19%**), $A^- - H_2O$ (240, **10%**), $A^- - CH_2OH$ (228, **9%**)
B^{2-}	$^{0,2}A_1^-$ (199, **100%**), $^{0,2}X_0^-$ (138, **59%**)	$B^{2-} - SO_3^-$ (256, **100%**), HSO_4^- (97, **48%**), SO_3^- (80, **22%**), m/z = 175 (**21%**), $B^{2-} - CH_2OSO_3^- - H_2O$ (210, **11%**), $^{0,2}X_0^-$ (138, **9%**), $B^{2-} - SO_3^- - H_2O$ (238, **7%**), $^{0,2}A_1^- - H_2O$ (178, **6%**), $^{0,2}A_1^-$ (199, **8%**), $B^{2-} - CH_2OSO_3^-$ (228, **4%**), $B^{2-} - e^-$ (338, **1%**)
C^{2-}	$C^{2-} - HSO_4^-$ (240, **100%**), HSO_4^- (97, **64%**)	HSO_4^- (97, **100%**), SO_3^- (80, **85%**), $C^{2-} - HSO_4^- - CH_2OH - H_2O$ (193, **60%**), m/z = 150.1 (**53%**), $^{0,3}X_0^-$ (247, **38%**), $C^{2-} - SO_3^-$ (259, **36%**), m/z = 178 (**34%**), $^{0,2}X_0^-$ (137, **25%**), m/z = 228 (**21%**), $C^{2-} - e^- - CH_2OH - H_2O$ (291, **11%**), $C^{2-} - e^- - CH_2OH$ (306, **11%**), $C^{2-} - HSO_4^-$ (240, **10%**), $C^{2-} - CH_2OH$ (153, **5%**), $^{0,3}X_0^{2-}$ (123, **3%**), $C^{2-} - HSO_4^- - CH_2OH$ (210, **3%**), $C^{2-} - e^-$ (338, **3%**)

[a] m/z values and fragment intensities (in bold, relative to the strongest fragment ion) are given in parentheses. Prominent, unassigned peaks are also included in the table, listed by their observed m/z values.

m/z = 175, although the low peak intensity indicates that glycosidic cleavage is a minor channel at low collision-energy.

The corresponding high-energy MIKE fragmentation spectrum (50 keV) of IVA^- is displayed in Fig. 6b. This spectrum displays the full complement of glycosidic fragments, with the C_1^- fragment ion now being the dominant product. In addition to the fragments associated with glycosidic cleavage (C_1^-, Z_1^-, B_1^-, Y_1^-), $^{0,2}A_1^-$, $^{0,2}A_2^-$ and $^{0,2}X_1^-$ fragment ions corresponding to cross-ring fragmentations are also clearly present. We note that negatively charged fragments are observed for all the possible glycosidic breakages (*i.e.*, fragments are observed without the carboxylate part of the molecule carrying the negative charge).

The low- and high-energy fragmentation mass spectra of the IH^{2-} dianionic disaccharide (α-ΔUA-2S-[1 → 4]-GlcN-6S) are displayed in Fig. 7. The most prominent fragmentation channel in the low-energy CID fragmentation spectrum (Fig. 7a) corresponds to a cross-ring cleavage that results in production of the $^{0,2}A_2^{2-}$ dianion (m/z = 218). Fragmentation of a dianion with production of a smaller dianion and a neutral fragment is unusual for relatively small molecular dianions, and is generally driven by the production of a stable neutral molecule [28]. For IH^{2-}, fragmentation along the $^{0,2}X_0$ cleavage produces $HNH_2C{=}CHOH$, consistent with this general picture. A C_1^- glycosidic-cleavage product ion (m/z = 255) is again evident as a minor fragment, along with an ion associated with loss of water from IH^{2-} (m/z = 238).

Upon high-energy collisional activation (Fig. 7b—100 keV), the IH^{2-} dianionic disaccharide primarily fragments with production of SO_3^- and HSO_4^-, mirroring the behavior of the B^{2-} and C^{2-} monosaccharides, which also possess OSO_3^- groups as charge carriers. The fragment ion corresponding to loss of SO_3^- from the parent dianion (m/z = 414) is also evident, indicating that the parent dianion fragments *via* a coulombic explosion. Like the B^{2-} monosaccharide, IH^{2-} shows less propensity to undergo both cross-ring and glycosidic cleavages. In fact, any such peaks appear within the noise level of the spectrum. The electron detachment fragment ion, $IH^{2-} - e^-$, again appears with very low intensity.

Fig. 8a displays the low-energy CID fragmentation spectrum for the IS^{3-} trianionic disaccharide (α-ΔUA-2S-[1 → 4]-GlcNS-6S) obtained at 6.5% relative CID energy. The major low-energy fragmentation channel for the trianionic parent ion corresponds to

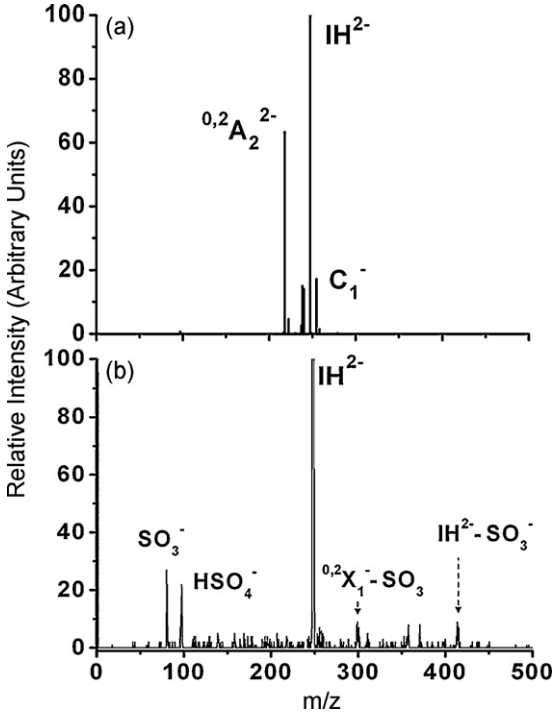

Fig. 7. (a) Low-energy CID mass spectrum of the IH^{2-} (*i.e.*, $[IH-2H]^{2-}$) dianionic monosaccharide at 7.9% collision energy. (b) Negative-ion MIKE spectrum (100 keV) following high-energy collision of IH^{2-} with Neon.

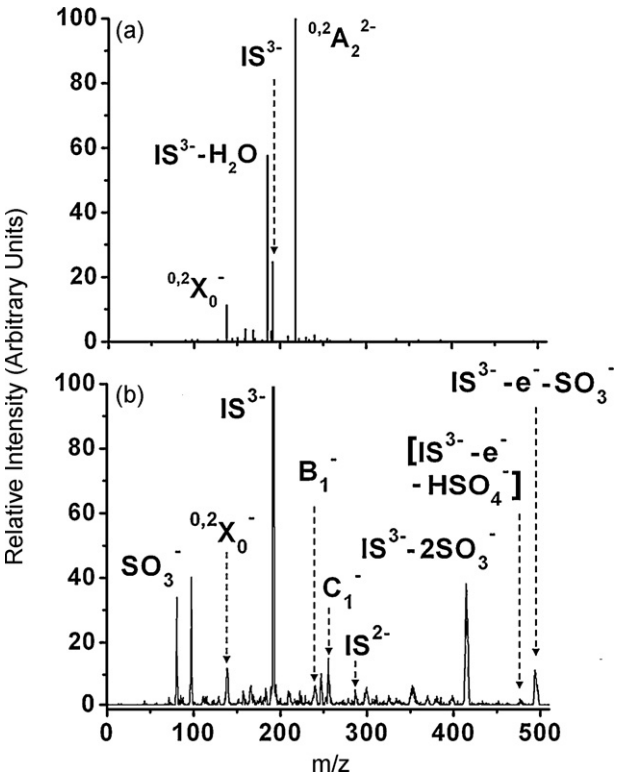

Fig. 8. (a) Low-energy CID mass spectrum of the IS^{3-} (*i.e.*, $[IS-3H]^{3-}$) trianionic monosaccharide at 6.5% collision energy. (b) Negative-ion MIKE spectrum (150 keV) following high-energy collision of IS^{3-} with Neon.

Table 2
Fragment ions present in the low- and high-energy fragmentation spectra of the IVA^-, IH^{2-} and IS^{3-} disaccharide anions, and the $Na^+{\cdot}IH^{2-}$ and $Na^+{\cdot}IS^{3-}$ sodiated complexes[a].

Parent Ion	Low-energy fragment ions	High-energy fragment ions
IVA^-	$^{0,2}A_2^-$ (277, **100%**), $^{0,2}X_1^-$ (259, **22%**), C_1^- (175, **5%**), $IVA^- - H_2O$ (360, **2%**)	C_1^- (175, **100%**), $^{0,2}X_1^-$ (258, **39%**), $^{0,2}A_2^-$ (277, **29%**), Y_1^- (217, **16%**), $^{0,2}A_1^-$ (115, **14%**), $IVA^- - H_2O$ (360, **7%**), $IVA^- - CH_2OH$ (346, **7%**), B_1^- (157, **7%**), Z_1^- (203, **2%**)
IH^{2-}	$^{0,2}A_2^{2-}$ (218, **100%**), C_1^- (255, **27%**), $IH^{2-} - H_2O$ (238, **24%**)	SO_3^- (80, **100%**), HSO_4^- (97, **82%**), $IH^{2-} - SO_3^-$ (414, **33%**), $^{0,2}X_1^- - SO_3$ (299, **33%**), m/z = 358 (**30%**), m/z = 370 (**30%**), C_1^- (255, **26%**), m/z = 311 (**19%**), $^{0,2}A_2^-$ (438, **8%**), $^{0,2}A_1^-$ (118, **7%**), $IH - e^- - CO_2$ (450, **7%**), $^{0,2}X_1^-$ (380, **7%**), $IH^{2-} - e^-$ (496, **4%**)
IS^{3-}	$^{0,2}A_2^{2-}$ (218, **100%**), $IS^{3-} - H_2O$ (185, **58%**), $^{0,2}X_0^-$ (138, **11%**)	HSO_4^- (97, **100%**), $IS^{3-} - 2SO_3^-$ (415, **95%**), SO_3^- (80, **84%**), C_1^- (256, **39%**), $^{0,2}X_0^-$ (139, **34%**), $IS^{3-} - SO_3^- - e^-$ (494, **27%**), $IS^{3-} - SO_3^-$ (247, **21%**), m/z = 352 (**15%**), $IS_3^- - SO_3^- - SO_3$ (166, **15%**), m/z = 300 (**14%**), $IS^{3-} - e^-$ (286, **11%**), $B_1^- - SO_3$ (158, **11%**), B_1^- (238, **7%**), $IS^{3-} - CO_2$ (176, **6%**), $IS^{3-} - e^- - HSO_4^- - SO_3$ (397, **5%**), $IS^{3-} - e^- - HSO_4^-$ (477, **4%**)
$Na^+{\cdot}IH^{2-}$	$Na^+{\cdot}{}^{0,2}A_2^{2-}$ (459, **100%**), $^{0,2}A_2^- - 2H_2O$ (402, **25%**), $^{0,2}A_2^-$ (438, **16%**), $Na^+{\cdot}IH^{2-} - H_2O$ (500, **7%**), $^{0,2}A_2^- - H_2O$ (420, **6%**)	$^{0,2}A_2^- - 2H_2O$ (401, **100%**), Y_1^- (258, **94%**), m/z = 342 (**72%**), m/z = 361 (**66%**), $Na^+{\cdot}\ IH^{2-} - CO_2$ (473, **65%**), IH^{2-} (248, **53%**), $Na^+{\cdot}{}^{0,2}A_2^{2-}$ (459, **53%**), m/z = 200 (**53%**), $^{0,2}A_2^{2-}$ (217, **50.0%**), m/z = 413 (**50%**), $IH^{2-} - H_2O$ (240, **34%**), $^{0,2}A_2^{2-}$ (459, **34%**), HSO_4^- (97, **25%**), SO_3^- (80, **19%**)
$Na^+{\cdot}IS^{3-}$	$Na^+{\cdot}{}^{0,2}A_2^{2-}$ (459, **100%**), $^{0,2}X_0^-$ (138, **19%**), m/z = 216 (**11%**), m/z = 531 (**7%**)	$Na^+{\cdot}IS^{3-} - SO_3^-$ (516, **100%**), $Na^+{\cdot}IS^{3-} - HSO_4^-$ (500, **14%**), $Na^+{\cdot}IS^{3-} - SO_3^- - CO_2$ (472, **13%**), m/z = 401 (**13%**), HSO_4^- (97, **10%**), $Na^+{\cdot}Z_1^{2-}$ (343, **8%**), $Na^+{\cdot}{}^{0,2}A_2^{2-}$ (459, **7%**), $IS^{3-} - 2SO_3^-$ (414, **7%**), m/z = 313 (**6%**), m/z = 200 (**6%**), $^{0,2}X_0^-$ (140, **6%**), m/z = 240 (**5%**), $Na^+{\cdot}Y_1^{2-}$ (360, **5%**), $Na^+{\cdot}B_1^{2-}$ (259, **5%**), SO_3^- (80, **4%**), B_1^{2-} (120, **4%**), $Na^+{\cdot}IS^{3-} - CO_2$ (277, **3%**), m/z = 533 (**3%**), $Na^+{\cdot}IS^{3-} - e^-$ (597, **1%**)

[a] m/z values and fragment intensities (in bold, relative to the strongest fragment ion) are given in parentheses. Prominent, unassigned peaks are also included in the table, listed by their observed m/z values.

ionic fragmentation *via* a cross-ring cleavage with production of the $^{0,2}X_0^-$ and $^{0,2}A_2^{2-}$ pair of anions. The fragmentation channel corresponding to loss of water from the parent ion is also prominent, while fragments associated with glycosidic cleavages are noticeably absent.

Finally, Fig. 8b displays the high-energy collision fragmentation spectrum (150 keV) of IS^{3-}. Coulomb explosion decay of the tri-anion is again evident in the prominent production of the SO_3^- and $[IS^{3-} - SO_3^-]$ fragment pair as in the MIKE spectra of IH^{2-}. The corresponding $[IS^{3-} - 2SO_3^-]$ fragment also appears as the major fragment ion. In contrast to the low-energy CID spectrum, the high-energy collision fragmentation spectrum shows both the C_1^- (m/z = 256) and B_1^- (m/z = 238) glycosidic product ions. The single cross-ring cleavage is also evident through the production of the $^{0,2}X_0^-$ fragment. The fragment ion corresponding to electron detachment, *i.e.*, $IS^{3-} - e^-$ (m/z = 286) again appears with only low intensity, although the fragment corresponding to electron detachment coupled with SO_3^- loss (*i.e.*, $IS^{3-} - e^- - SO_3^-$ m/z = 494) appears more prominently. A minor fragment corresponding to electron loss accompanied by HSO_4^- loss (*i.e.*, $IS^{3-} - e^- - HSO_4^-$ m/z = 477) is also present at low intensity. A full list of fragments observed in the low- and high-energy fragmentation spectra for the disaccharides studied is given in Table 2, with assignments.

3.3. Sodiated clusters of the IH^{2-} and IS^{3-} disaccharides

To compare the fragmentation patterns observed, the sodiated clusters of the IH^{2-} and IS^{3-} disaccharides were also investigated using the high-energy collision technique. Fig. 9 displays the low-energy (21.4% CID energy) and high-energy fragmentation spectra for $Na^+{\cdot}IH^{2-}$. The most prominent fragment in the low collision-energy spectrum (Fig. 9a) corresponds to loss of the neutral $^{0,2}X_0$ fragment from the parent cluster, producing $Na^+{\cdot}{}^{0,2}A_2^{2-}$ (m/z = 439). This behavior mirrors the low-energy fragmentation patterns of other dianion-cation complexes we have investigated [36–38], where fragmentation of the cluster occurs by the same pathway as for the bare dianion. The high-energy MIKE spectrum is shown in Fig. 9b, and displays much higher signal/noise than the corresponding unsodiated spectrum (Fig. 7b). As in the low-energy spectrum, a product ion is evident at m/z = 459 corresponding to loss of neutral $^{0,2}X_0$ from the parent ion. In addition, the high-energy spectrum displays a Y_1^- glycosidic fragmentation product ion. Loss of Na^+ from the parent ion is evident through the appearance of IH^{2-} (m/z = 248).

Finally, the $Na^+{\cdot}IS^{3-}$ low- and high-energy fragmentation mass spectra are displayed in Fig. 10. Low-energy fragmentation of $IS^{3-}{\cdot}Na^+$ (Fig. 10a) occurs with production of the $^{0,2}X_0^-$ and $Na^+{\cdot}{}^{0,2}A_2^{2-}$ pair of fragments, indicating that the multiply charged anion, IS^{3-}, is again fragmenting within the cluster by the same pathway as for the bare ion. This behavior reflects the fact that the sodiated sugar complexes are true ion-pairs, [36–38] where the counterion only weakly perturbs the electronic structure of the multiply charged saccharide anion. The $^{0,2}X_0^-$ and $Na^+{\cdot}{}^{0,2}A_2^{2-}$ pair of fragments are again evident in the high-energy MIKE spectrum (Fig. 10b), along with a variety of other product ions corresponding

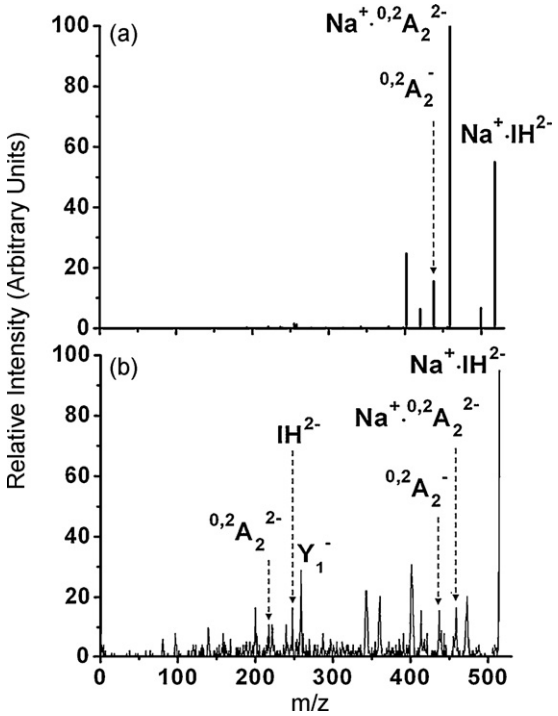

Fig. 9. (a) Low-energy CID mass spectrum of the $Na^+{\cdot}IH^{2-}$ sodiated cluster at 21.4% collision energy. (b) Negative-ion MIKE spectrum (50 keV) following high-energy collision of $Na^+{\cdot}IH^{2-}$ with Neon.

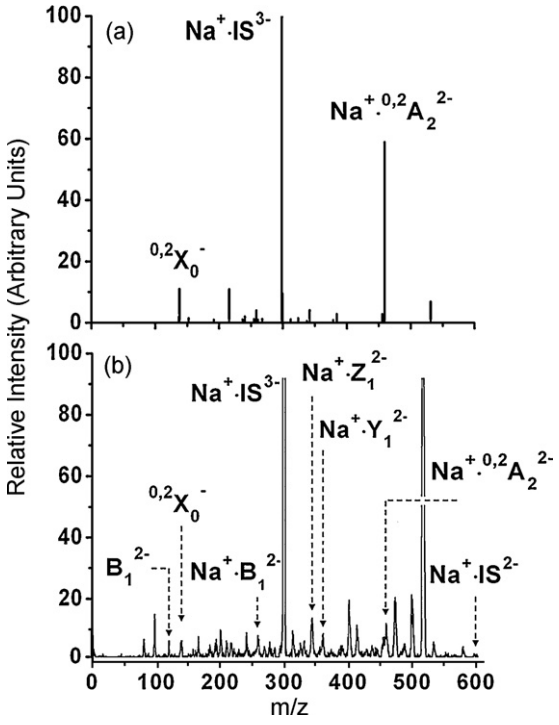

Fig. 10. (a) Low-energy CID mass spectrum of the $Na^+ \cdot IS^{3-}$ sodiated cluster at 10.7% collision energy. (b) Negative-ion MIKE spectrum (100 keV) following high-energy collision of $Na^+ \cdot IS^{3-}$ collision with Neon.

to both C_1 and B_1 glycosidic ring cleavages. Once again, the fragment ion corresponding to electron detachment from the $Na^+ \cdot IS^{3-}$ parent dianion is a very minor fragment.

The variety of fragment ions observed in the high-energy spectra of the $Na^+ \cdot IS^{3-}$ sodiated complex is of key interest, since they suggest that the three excess charges in IS^{3-} are distributed across the four acidic groups. For example, the occurrence of the $B_1{}^{2-}$ fragment indicates that excess charges are located on the carboxylate and sulphate group of the B_1 ring in some of the disaccharides, while the $Na^+ \cdot Z_1{}^{2-}$ and $Na^+ \cdot Y_1{}^{2-}$ fragments indicate that excess charges are located on the sulphate and $NHSO_3$ groups of the Z_1 ring. The simplest explanation of these observations is that the excess charges are distributed across the four acidic groups, and the high-energy experiment on the sodiated cluster therefore provides insight into the charge localization in the trianion. We note that the distribution of charge across the four acidic groups of IS is initially surprising given that the pK_a value of the carboxyl group is higher (~5) [39] than the value for a $-OSO_3H$ or $-NHSO_3H$ group (0.25 and 1.0, respectively) [40–42]. However, Tian and Kass have recently studied the deprotonation sites of the gas-phase tyrosine monoanion (carboxylate or phenoxide), and have found that deprotonation is highly dependent on the electrospray solvent used to spray the anion [43].

The high-energy fragmentation behavior of the $Na^+ \cdot IS^{3-}$ system is notably different from the analogous $Na^+ \cdot IH^{2-}$ cluster where only the $Y_1{}^-$ glycosidic fragment is observed. This may be due to the presence of an NH_2 group at the C2 position of IH^{2-}, where IS^{3-} has an acidic $NHSO_3H$ group. A full list of fragments, with assignments, is given in Table 2 for the sodiated clusters of IH^{2-} and IS^{3-}.

4. Discussion

In general, the anionic monosaccharides and disaccharides investigated in this work fragment along pathways that are primarily determined by their excess charges. In the low-energy CID studies, the monoanions are relatively stable compared to the multiply charged saccharides which fragment at much lower relative collision energies. This reflects the intrinsic instability of small, multiply charged molecular ions in the gas-phase. In both the high-energy and low-energy collision experiments, the dianionic and trianionic saccharides are susceptible to fragmenting *via* Coulombic explosion, which is typically the lowest barrier pathway for activated decay of gas-phase multiply charged anions.

Decay *via* electron detachment of the multiply charged saccharide anions is also evident in the high-energy collision experiments. This contrasts with the low-energy CID experiments, where electron detachment from small multiply charged anions is not generally observed [28]. Initial electron loss is often followed by further fragmentation, leading to ions that are not formed in low-energy CID. One of the striking features about the data obtained for the multiply charged saccharide anions is that the electron detachment fragment ions appear with very low intensity, in contrast to other multiply charged anions that have been studied in high-energy collision experiments [16–21]. For example, in a study of the $[d(A)_x - nH]^{n-}$ ($x = 7.5$ and $n = 1$–6) oligonucleotides, the single electron loss fragment ions were dominant in the fragment ion mass spectrum [20].

The low intensity of the electron detachment fragments for the multiply charged saccharide anions is likely due to the fact that these systems are susceptible to further rapid fragmentation following electron loss. It is useful, in this context to compare the high-energy collision results obtained here with electron detachment dissociation results for similar systems [22,44]. In EDD experiments on $[M-2H]^{2-}$ sulphated sugars, the electron detachment product ions are indeed also small, a fact that was attributed to electron loss occurring from the sulphate group, leaving a sulphate radical that is susceptible to SO_3 loss. This loss channel would appear to be evident in the systems studied here where fragment ions are observed corresponding to loss of an $SO_3{}^-$ unit (equivalent to loss of e^- followed by loss of neutral SO_3) [45]. It is interesting to note that in EDD experiments on sugars that contained deprotonated carboxylate and sulphate groups, no electron loss was observed from the sulphate group. Electron loss, followed by decarboxylation, is thought to occur preferentially from the carboxylate group since the electron binding energy of sulphate is considerably higher than that of carboxylate. In the high-energy collisions studied here, however, systems such as IH^{2-} with both deprotonated carboxylates and sulphate groups, do not decay preferentially by electron loss followed by decarboxylation, presumably due to the higher energy available in the collision. This illustrates one way in which the high-energy CID experiments performed in this study can complement EDD measurements.

The fragmentation patterns of the sodiated-multiply charged sugar clusters are characteristic of smaller cation-dianion clusters that we have studied previously [36–38]. In these simpler complexes (*e.g.*, $K^+ \cdot Pt(CN)_4{}^{2-}$), the cluster fragmentation is characteristic of the dianion, for example when the dianion fragments with production of $Pt(CN)_3{}^-$ and CN^-,

$$Pt(CN)_4{}^{2-} | Pt(CN)_3{}^- + CN^- \quad (1)$$

the related cation-dianion cluster fragments as follows,

$$K^+ \cdot Pt(CN)_4{}^{2-} | Pt(CN)_3{}^- + K^+ \cdot CN^- \quad (2)$$

These results indicate that the electronic structure of the dianion is not significantly perturbed within the cation-dianion complex and hence the clusters represent true ion-pairs. Since the sodiated-multiply charged sugar clusters studied here also appear to correspond to ion-pairs, it is reasonable to assume that similar sodiated-anionic sugar complexes will fragment in a manner that can be straightforwardly interpreted. This could be useful from an analytical perspective since sodiated-anionic sugar complexes are frequently more dominant in ESI-MS than the unsodiated analogues,

[47] and are intrinsically more robust due to the reduced overall charge of the complex.

Unsurprisingly, high-energy collisional activation does produce a greater number of fragment ions than low-energy CID. This should be beneficial for obtaining diagnostic information about the saccharide structures, but the nature of the fragment ions is also important. In particular, it is desirable that the fragment ions retain the crucial sulphate groups. The high-energy results obtained in this study are promising in this respect. For the A, B^{2-}, and C^{2-} monosaccharides, the high-energy fragmentation mass spectra display ions associated with cross-ring fragmentation with retained sulphate groups. In addition, the $^{0,3}X_0^-$ cross-ring fragment is also evident for C^{2-} but not for B^{2-}. This is of particular interest since it suggests that this fragment may represent a high-energy diagnostic fragment for identifying the location of the sulphate group. The presence of the $^{0,2}X_0^-$ fragment in both the B^{2-} and C^{2-} spectra demonstrates the general utility of the high-energy technique, since it is present irrespective of the sulphate position and without loss of the sulphate group.

Another example of the diagnostic utility of the high-energy fragmentation technique for providing crucial structural information is illustrated by the IH^{2-} disaccharide results. This molecular anion shares its m/z value with the related IIS^{2-} and $IIIS^{2-}$ Heparin sub-units, which are often found together in mixtures with IH^{2-} [48]. Low-energy CID of IH^{2-} results in production of $^{0,2}A_2^{2-}$ as the major fragment ion, along with C_1^- (glycosidic cleavage) and $[IH^{2-}–H_2O]$, a set of fragments that are insufficient to structurally characterize the disaccharide. In contrast, the high-energy spectrum of IH^{2-} displays singly charged $^{0,2}A_1^-$ and $^{0,2}X_1^-$ cross-ring fragments, which are highly diagnostic since they reveal the placement of the sulphate group on the uronic acid.

5. Summary

The high-energy collision results for anionic monosaccharides and disaccharides presented in this work illustrate that significantly more structural information can be obtained to characterize the saccharide structures compared to low-energy CID. The fragmentation patterns observed also appear to provide important complementary information to electron detachment dissociation measurements. More generally, the MIKE results illustrate how the application of novel molecular physics techniques can be useful for characterizing the structures of gas-phase biological ions, supplementing more traditional mass spectrometric techniques.

Acknowledgements

This experiment was performed at the Department of Physics and Astronomy, Aarhus University, part of the distributed LEIF infrastructure. The support received from the European Project ITS LEIF (R113/026015) is gratefully acknowledged. CEHD also thanks the EPSRC for support from Grant EP/C51212X/1, the Royal Society for support from a University Research Fellowship, and the ERC for support from grant 208589-BIOIONS. SBN gratefully acknowledges support from Lundbeckfonden, the Danish Natural Science Research Council (grant #272-06-0427), and Carlsbergfondet (grant #2006-01-0229).

References

[1] E.G. Robertson, J.P. Simons, Phys. Chem. Chem. Phys. 3 (2001) 1.
[2] T. Wyttenbach, M.T. Bowers, Top. Curr. Chem. 225 (2003) 207.
[3] P.E. Barran, N.C. Polfer, D.J. Campopiano, D.J. Clarke, P.R.R. Langridge-Smith, R.J. Langley, J.R.W. Govan, A. Maxwell, J.R. Dorin, R.P. Millar, M.T. Bowers, Int. J. Mass Spectrom. 240 (2005) 273.
[4] E. Nir, I. Hünig, K. Kleinermanns, M.S. de Vries, Phys. Chem. Chem. Phys. 5 (2003) 4780.
[5] M. Gerhards, C. Unterberg, A. Gerlach, A. Jansen, Phys. Chem. Chem. Phys. 6 (2004) 2682.
[6] S. Ullrich, G. Tarczay, X. Tong, C.E.H. Dessent, K. Müller-Dethlefs, Angew. Chem. Int. Ed. 41 (2002) 166.
[7] X. Tong, S. Ullrich, C.E.H. Dessent, K. Müller-Dethlefs, Phys. Chem. Chem. Phys. 4 (2002) 3578.
[8] J.A. Stearns, S. Mercier, C. Seaiby, M. Guidi, O.V. Boyarkin, T.R. Rizzo, J. Am. Chem. Soc. 129 (2007) 11814.
[9] S. Wiedemann, A. Metsala, D. Nolting, R. Weinkauf, Phys. Chem. Chem. Phys. 6 (2004) 2641.
[10] S. Brøndsted Nielsen, J.U. Andersen, P. Hvelplund, B. Liu, S. Tomita, J. Phys. B-At. Mol. Opt. Phys. 37 (2004) R25.
[11] S. Denifl, F. Zappa, A. Mauracher, F.F. daSilva, A. Bacher, O. Echt, T.D. Mark, D.K. Bohme, P. Scheier, ChemPhysChem 9 (2008) 1387.
[12] F. Alvarado, J. Bernard, B. Li, R. Bredy, L. Chen, R. Hoekstra, S. Martin, T. Schlatholter, ChemPhysChem 9 (2008) 1254.
[13] T. Schlathölter, F. Alvarado, S. Bari, A. Lecointre, R. Hoekstra, V. Bernigaud, B. Manil, J. Rangama, B. Huber, ChemPhysChem 7 (2006) 2339.
[14] B.P. Marinković, F. Blanco, D. Šević, V. Pejčev, G. Garcia, D.M. Filipović, D. Pavlović, N.J. Mason, Int. J. Mass Spectrom. 277 (2008) 300.
[15] R.J. Linhardt, T. Toida, Acc. Chem. Res. 37 (2004) 431.
[16] A.B. Nielsen, P. Hvelplund, B. Liu, S. Brøndsted Nielsen, S. Tomita, J. Am. Chem. Soc. 125 (2003) 9592.
[17] M.O. Larsson, P. Hvelplund, M.C. Larsen, H. Shen, H. Cederquist, H.T. Schmidt, Int. J. Mass Spectrom. 177 (1998) 51.
[18] R.M. Burke, W.E. Boxford, S. Panja, S. Brøndsted Nielsen, C.E.H. Dessent, Chem. Phys. Lett. 442 (2007) 201.
[19] W.E. Boxford, M.O.A. El Ghazaly, C.E.H. Dessent, S. Brøndsted Nielsen, Int. J. Mass Spectrom. 244 (2005) 60.
[20] B. Liu, P. Hvelplund, S. Brøndsted Nielsen, S. Tomita, Int. J. Mass Spectrom. 230 (2003) 19;
P. Hvelplund, B. Liu, S. Brøndsted Nielsen, S. Panja, J.-C. Poully, K. Støchkel, Int. J. Mass Spectrom. 263 (2007) 66.
[21] S.Y. Ovchinnikov, J. Macek, A.A. Tuiman, J.D. Steill, R.N. Compton, P. Hvelplund, A.I.S. Holm, S. Brøndsted Nielsen, M.B. Nielsen, Phys. Rev. A 73 (2006) 064704.
[22] J.J. Wolff, I.J. Amster, L. Chi, R.J. Lindhardt, J. Am. Soc. Mass Spectrom. 18 (2007) 234.
[23] J.J. Wolff, L. Chi, R.J. Linhardt, I.J. Amster, Anal. Chem. 79 (2007) 2015.
[24] J.T. Adamson, K. Håkansson, Anal. Chem. 79 (2007) 2901.
[25] A. Varki, R. Cummings, J. Esko, H. Freeze, G. Hart, J. Marth, Essentials of Glycobiology, Cold Spring Harbor Laboratory Press, 1999.
[26] O.M. Saad, J.A. Leary, Anal. Chem. 75 (2003) 2985.
[27] W.E. Boxford, J.K. Pearce, C.E.H. Dessent, Chem. Phys. Lett. 399 (2004) 465.
[28] W.E. Boxford, C.E.H. Dessent, Phys. Chem. Chem. Phys. 8 (2006) 5151.
[29] K.X. Wan, M.L. Gross, T. Shibue, J. Am. Soc. Mass Spectrom. 11 (2000) 450.
[30] J. Zhang, J.S. Brodbelt, J. Wang, J. Am. Soc. Mass Spectrom. 16 (2005) 139.
[31] B. Domon, C.E. Costello, Glycoconjugate J. 5 (1988) 397.
[32] O.M. Saad, J.A. Leary, J. Am. Soc. Mass Spectrom. 15 (2004) 1274.
[33] R.M. Burke, J.K. Pearce, W.E. Boxford, A. Bruckmann, C.E.H. Dessent, J. Phys. Chem. A 109 (2005) 9775.
[34] M.K. Scheller, R.N. Compton, L.S. Cederbaum, Science 270 (1995) 116.
[35] D. Schröder, Ang. Chem. Int. Ed. 43 (2004) 1329.
[36] R.M. Burke, W.E. Boxford, C.E.H. Dessent, J. Chem. Phys. 126 (2007) 064308.
[37] R.M. Burke, W.E. Boxford, C.E.H. Dessent, J. Chem. Phys. 125 (2006) 021105.
[38] W.E. Boxford, R.M. Burke, C.E.H. Dessent, Phys. Scripta 76 (2007) C56.
[39] D.R. Hide (Ed.), Handbook of Chemistry and Physics, CRC Press, Boca Raton, 2000.
[40] E.P. Serjeant, B. Dempsey, Ionization Constants of Organic Acids in Solution, Iupac Chemical Data Series No. 23, Pergamon Press, Oxford, U.K., 1979.
[41] H.P. Hopkins, C.H. Wu, L.G. Hepler, J. Phys. Chem. 69 (1965) 2244.
[42] The quoted pk_a values are for bulk aqueous solution. The gas-phase pk_as are unavailable for these species. Ref [43] discusses the issue of solution versus gas-phase deprotonation in electrospray.
[43] Z.X. Tian, S.R. Kass, J. Am. Chem. Soc. 130 (2008) 10842.
[44] J.J. Wolff, T.N. Laremore, A.M. Busch, R.J. Linhardt, I.J. Amster, J. Am. Soc. Mass Spectrom. 19 (2008) 790.
[45] The product ion peaks corresponding to loss of SO_3^- from parent ions that are observed in our MIKE experiments may correspond to loss of either an SO_3^- ion from the parent or for electron detachment followed by loss of neutral SO_3. We anticipate that both processes occur: the fragment ions corresponding to electron detachment from the parent appear with such low intensity, implying that e^-+SO_3 loss is common. We also observe the SO_3^- ion as a product ion, suggesting that direct SO_3^- loss occurs. However, the kinetic energy release for formation of SO_3^- and the corresponding (parent ion–SO_3^-) fragment ion is low, [46] which indicates that this pair of anions are not formed in the same dynamical process.
[46] G. Bojesen, P. Hvelplund, T.J.D. Jørgensen, S. Brøndsted Nielsen, J. Chem. Phys. 113 (2000) 6608.
[47] L. Jin, P.E. Barran, J.A. Deakin, M. Lyon, D. Uhrĩn, Phys. Chem. Chem. Phys. 7 (2005) 3464.
[48] J.R. Behr, Y. Matsumoto, F.M. White, R. Sasisekharan, Rapid Commun. Mass Spectrom. 19 (2005) 2553.